AGU PUBLICATIONS

Geophysical Research Letters

RESEARCH LETTER
10.1002/2016GL069154

Special Section:
First results from NASA's Magnetospheric Multiscale (MMS) Mission

Multispacecraft observations and modeling of the 22/23 June 2015 geomagnetic storm

P. H. Reiff[1], A. G. Daou[1], S. Y. Sazykin[1], R. Nakamura[2], M. R. Hairston[3], V. Coffey[4], M. O. Chandler[4], B. J. Anderson[5], C. T. Russell[6], D. Welling[7], S. A. Fuselier[8,9], and K. J. Genestreti[8,9]

[1]Rice Space Institute, Rice University, Houston, Texas, USA, [2]Space Research Institute, Austrian Academy of Sciences, Graz, Austria, [3]Center for Space Sciences, University of Texas at Dallas, Richardson, Texas, USA, [4]Marshall Space Flight Center, Huntsville, Alabama, USA, [5]The Johns Hopkins University Applied Physics Laboratory, Laurel, Maryland, USA, [6]IGPP, University of California, Los Angeles, California, USA, [7]Department of Atmospheric, Oceanic and Space Sciences, University of Michigan, Ann Arbor, Michigan, USA, [8]Southwest Research Institute, San Antonio, Texas, USA, [9]Physics and Astronomy Department, University of Texas at San Antonio, San Antonio, Texas, USA

Abstract The magnetic storm of 22–23 June 2015 was one of the largest in the current solar cycle. We present in situ observations from the Magnetospheric Multiscale Mission (MMS) and the Van Allen Probes (VAP) in the magnetotail, field-aligned currents from AMPERE (Active Magnetosphere and Planetary Electrodynamics Response), and ionospheric flow data from Defense Meteorological Satellite Program (DMSP). Our real-time space weather alert system sent out a "red alert," correctly predicting *Kp* indices greater than 8. We show strong outflow of ionospheric oxygen, dipolarizations in the MMS magnetometer data, and dropouts in the particle fluxes seen by the MMS Fast Plasma Instrument suite. At ionospheric altitudes, the AMPERE data show highly variable currents exceeding 20 MA. We present numerical simulations with the Block Adaptive Tree-Solarwind - Roe - Upwind Scheme (BATS-R-US) global magnetohydrodynamic model linked with the Rice Convection Model. The model predicted the magnitude of the dipolarizations, and varying polar cap convection patterns, which were confirmed by DMSP measurements.

Key Points:
- MHD models can reproduce well the dipolarizations seen at MMS and VAP. Space weather forecasting can predict *Kp* variations within 0.5 step
- Beams of O^+ flowing downstream appear to cross the separatrix and become a second energized population of the tail plasma sheet
- MHD models successfully reproduced the polar cap convection patterns and cross-polar cap potential drops for a range of IMF conditions

Supporting Information:
- Supporting Information S1
- Figure S1
- Movie S1
- Movie S2
- Movie S3
- Movie S4

Correspondence to:
P. H. Reiff,
reiff@rice.edu

Citation:
Reiff, P. H., et al. (2016), Multispacecraft observations and modeling of the 22/23 June 2015 geomagnetic storm, *Geophys. Res. Lett.*, *43*, 7311–7318, doi:10.1002/2016GL069154.

Received 13 APR 2016
Accepted 21 MAY 2016
Accepted article online 25 MAY 2016
Published online 20 JUL 2016

1. Introduction

On 22 June, one moderate and one giant coronal mass ejection (CME) passed the ACE spacecraft at 04:51 and 17:58 UT, respectively. The larger shock was observed by the magnetometer instrument [*Smith et al.*, 1998] as a jump in the interplanetary magnetic field (IMF) from about 10 to over 40 nT and by the Solar Wind Electron, Proton, and Alpha Monitor (SWEPAM) instrument [*McComas et al.*, 1998] as a jump in solar wind density from 20 to over 45 particles/cm^3, with a corresponding increase in pressure to over 50 nPa. When propagated to the bow shock, it was forecast to impact at about 18:36 UT after a smaller shock at about 05:40 UT (Figure 1a). Coupled with a strong southward IMF (Figure 1d), the Boyle Index reached nearly 500 kV, prompting our forecast system (http://mms.rice.edu/realtime/forecast.html) to send out a "yellow alert" at 06:04 and a "red alert" at 18:34, even before the CME impacted the bow shock. The *y* component of the IMF was very strong, with the IMF clock angle (Figure 1e), rotating anticlockwise then clockwise nearly 360°. The neural network forecaster [*Bala and Reiff*, 2012] predicted *Kp* of over 8 and the *Kp* forecast status went to "red" at 19:02.

The magnetospheric flotilla of spacecraft included Magnetospheric Multiscale Mission (MMS), Van Allen Probes (VAP), Time History of Events and Macroscale Interactions during Substorms (THEMIS), and Cluster in the magnetosphere, plus AMPERE, Defense Meteorological Satellite Program (DMSP), and the International Space Station (ISS) at low altitudes. This paper will concentrate on the large-scale features of the activity. It will include selected MMS, VAP, AMPERE, and DMSP results and compare to the BATS-R-US model simulations. Other papers in this issue [e.g., *Baker et al.*, 2016; *Nakamura et al.*, 2016] will focus on other aspects of this event.

2. Space Weather Forecasting

The Rice University space forecast system (http://mms.rice.edu/realtime/forecast.html) predicts the *Kp*, *AE*, and *Dst* indices for 1 and 3 h ahead of real time, at a cadence of 15 m. The prediction is based on a neural network forecast that uses one or more base functions and lookback data of up to 24 h. Yellow alerts are sent out if the forecast *Kp* is greater than 4, and red alerts if the forecast *Kp* is 6 or greater [*Bala and Reiff*, 2012]. Statistically, the accuracy of the predicted *Kp* is approximately one unit. Three base formulas are used in the forecast:

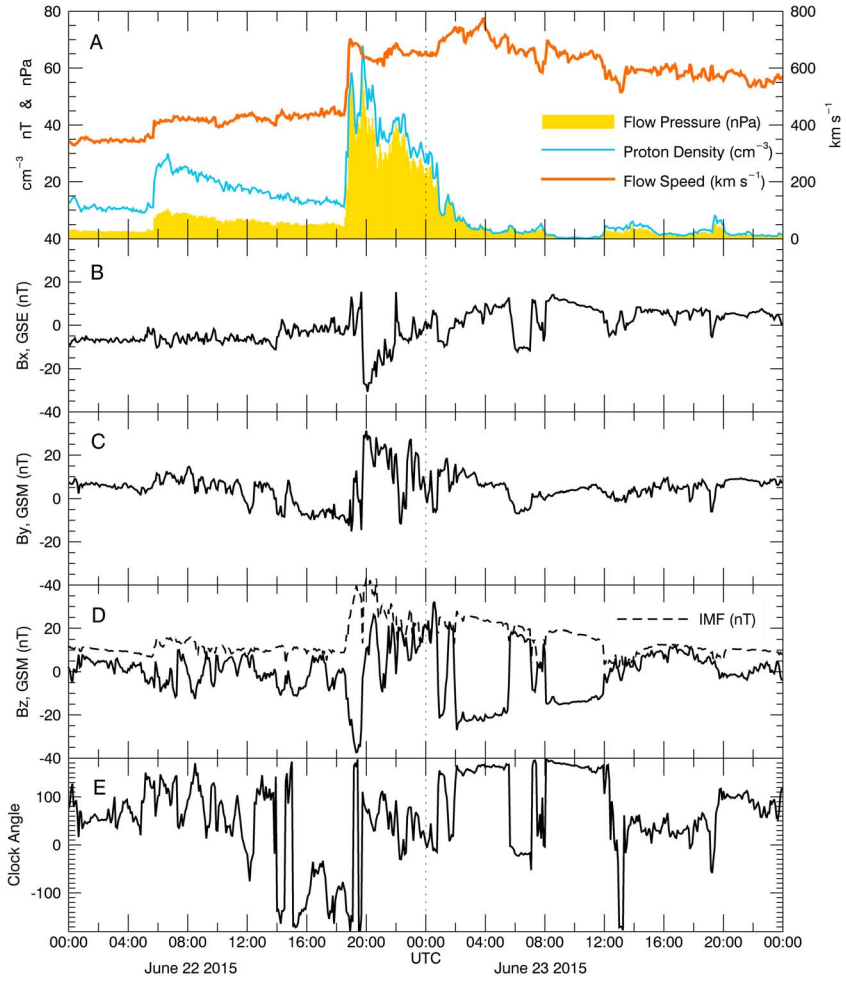

Figure 1. Interplanetary conditions during the event. (a) Solar wind density, velocity, and flow pressure; (b–d) IMF B_x, B_y, B_z (and $|B|$ shown dashed) components (GSM); (e) IMF clock angle (0 = $+B_z$; 90 = $+B_y$ direction). The values are plotted from OMNI data, propagated to the bow shock.

the Boyle Index (marked as BI), the Boyle Index with a ram pressure term (RAM), and the Newell function (Newell) [*Bala and Reiff*, 2014]. All have similar prediction efficiencies, and the three predictions generally span the actual measured quantities. For this event, all three formulas gave similar predictions, with the *AE* index least well predicted ($r = 0.61$ to 0.72), whereas *Kp* and *Dst* were successful with $r = 0.79$ to 0.91 (Figure 2).

A comment on timing of "predictions" is in order. The forecast algorithm was trained on 1 h averages of *AE*, *Dst*, and *Kp**, with the *Kp** values being an overselection of *Kp* (because it is intrinsically a 3 h average). The algorithm predicts the 1 h *AE*, *Dst*, and *Kp** values for the hour following, based on the solar wind data of the previous hour. The calculation is done at the top of the hour after the real-time solar wind data are received, and a forecast typically posted at 6 min past the hour for the hour of the forecast (e.g. 18:06 for the hours 18–19). In this case, because the shock hit at the very end of hour 17, the *AE* predictions for hours 18–19 were not as high as the provisional *AE* turned out to be (Figure 2c), because the forecast only included 2 min of postshock data and because the high solar wind speed meant that the shock arrived at Earth well before the end of hour 18. The forecast 3 h *Kp*, based on 3 h averages of the 1 h predictions (Figure 2a), does show a very good fit ($r = 0.88$ to 0.91, implying an accuracy of prediction from 0.36 to 0.47 step in *Kp*).

3. Magnetotail Observations

Since the MMS spacecraft suite [*Burch et al.*, 2016] was in the "commissioning" phase of its mission, not all of the instruments were fully operational. All of the magnetometers [*Russell et al.*, 2016] and many of the particle

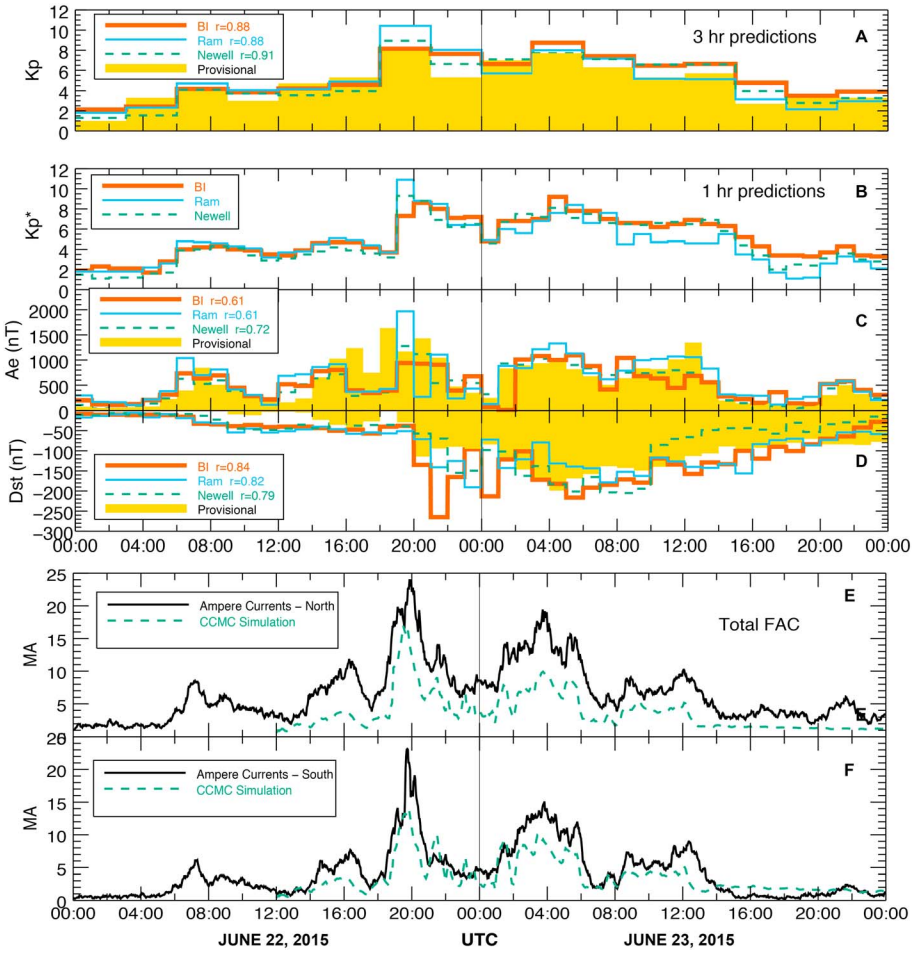

Figure 2. Comparison of predicted and modeled values compared to data. (a) The predicted 3 h *Kp* index for 22–23 June 2015, compared to the provisional *Kp*, with a 90% correlation coefficient. Predicted (histograms) and observed provisional (yellow) (b) *Kp**, (c) *AE*, and (d) *Dst* indices. All three base functions: BI (thick line), Ram (thin line), and Newell (dashed) performed well, some slightly better than others. Modeled integrated field-aligned currents (dashed) versus those calculated from AMPERE measurements for the (e) Northern and (f) Southern Hemispheres.

detectors were making measurements and saw the dynamic response of the magnetosphere. The Fast Plasma Instrument (FPI) on board MMS2 [*Pollock et al.*, 2016] saw a number of excursions between the plasma sheet and the lobe, shown in Figure 3 as particle flux dropouts at about 3:20–3:30 and 5:11–05:40 UT (Figures 3c and 3d). Clearly visible in the lobe are antisunward flowing ions, at a few hundred eV (Figures 3b and 3c). The Hot Plasma Composition Analyzer (HPCA) on board MMS1 [*Young et al.*, 2016] identified these beams as O^+ (Figure 3b) presumably from auroral outflow [*Lu et al.*, 1992] or possibly from the dayside cusp [*Liao et al.*, 2010] though cusp ions will more likely reach the neutral sheet farther downtail [*Liao et al.*, 2012]. The HPCA instrument, because of a new AC sweep field, can reduce background H^+ fluxes by nearly 2 orders of magnitude, making the determination of the heavy ion species much more reliable. This cool lobe ion beam appears to be accelerated and heated as it crosses into the plasma sheet. In Figures 3e–3g, we show sample total ion particle distributions from FPI MMS2 as the spacecraft exits the plasma sheet into the lobe around 05:10:30. In the lobe around 05:11:19 (Figure 3g), we see two separated cold ion beams: one with a parallel velocity of around 50 km/s and another with a parallel velocity of ~200 km/s. The right image of that pair shows that those beams are also convecting at about the same $\mathbf{E}\times\mathbf{B}$ speed (v_{perp1}) as the parallel speeds, with no drift in the other direction (v_{perp2}) perpendicular to Figure 3b. From the HPCA data (Figures 3a and 3b), it is clear that the less energetic ions are H^+ and the ones with apparently higher velocity are just O^+ ions with the same parallel and perpendicular velocity as the H^+ ions. This is confirmed by the HPCA particle distribution plots (not shown). As the spacecraft exits

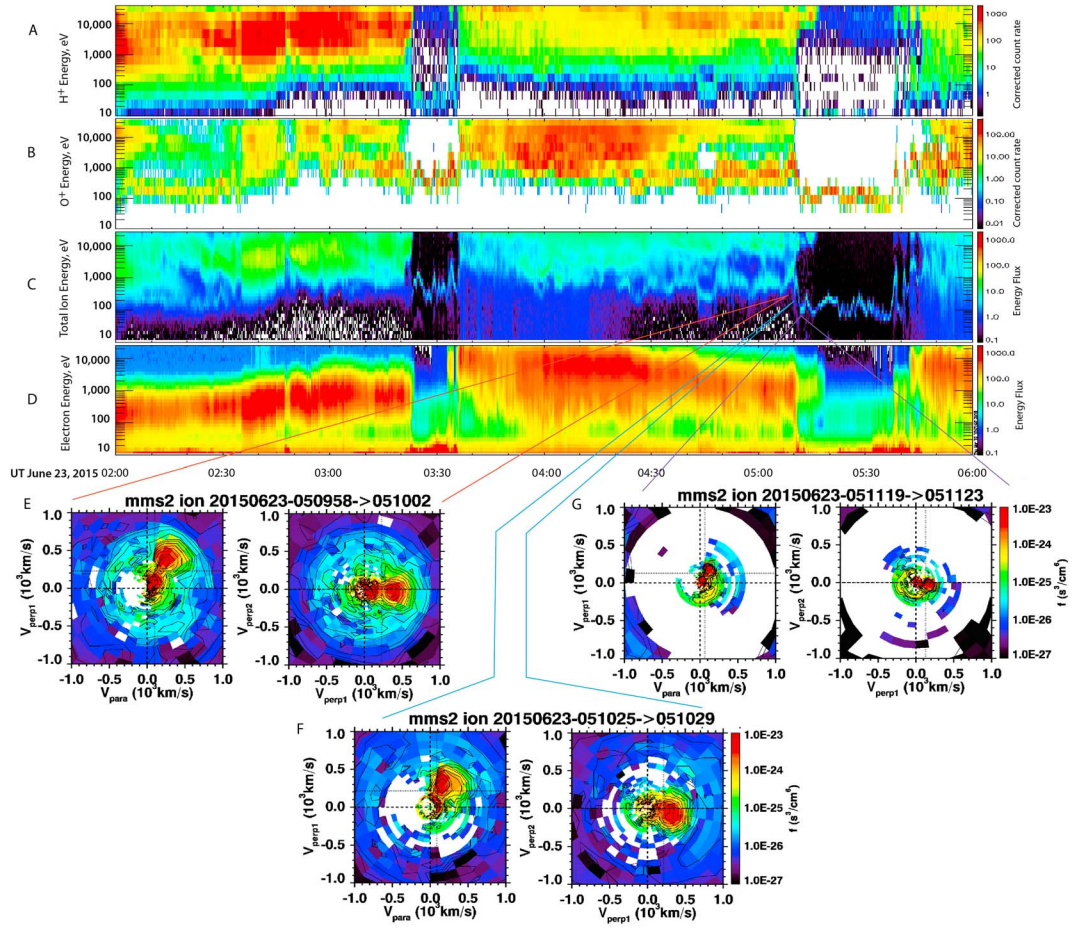

Figure 3. HPCA (MMS1) and FPI (MMS2) measurements in the magnetotail from 0200 to 0600 on 23 June. Energy spectrograms of the HPCA (a) H^+ and (b) O^+ corrected counts are shown with Figure 3b showing an O^+ beam from the ionosphere merging into the plasma sheet at each lobe/plasma sheet transition. (c) FPI ion and (d) electron spectrograms of differential energy flux are shown. (e–g) Three pairs of FPI distribution functions as the spacecraft exited the plasma sheet to the lobe. (left) The $v_{parallel}$ and v_{perp1} (along $\mathbf{E}\times\mathbf{B}$) components of the particle distribution functions and (right) the two perpendicular velocities, v_{perp1} and v_{perp2}. Similar distribution functions from HPCA are shown in the supporting information.

the plasma sheet boundary layer at around 05:10:30 (Figure 3f), we see the same two beams, but now with a $\mathbf{E}\times\mathbf{B}$ velocity double that in the lobe, This middle distribution does show some v_{perp2}, but it is not clear whether this is a time aliasing as the fields change direction during the 4 s measurement of the distribution function. The distribution function measured deepest in the plasma sheet (Figure 3e, at 05:09:58) shows the highest parallel and $\mathbf{E}\times\mathbf{B}$ drift speeds, and no significant v_{perp2}. For additional information on this event, see *Nakamura et al.* [2016].

At the same time, the magnetic fields observed at MMS in the tail and by VAP closer to the Earth showed dramatic dipolarizations as the magnetotail responded to the northward turnings of the IMF (Figure 4). At MMS-1 (Figure 4, top), the measured B_x went from −90 to −20 nT, and B_z increased from near 0 to 30 nT. The transitions from MMS from the plasma sheet to the lobe resulted primarily because of the thinning and expansion of the plasma sheet and partially because of the flapping of the magnetotail current sheet up and down.

4. Modeling Results

To put these observations into context, we ran the BATS-R-US model [*Powell et al.*, 1999; *Tóth et al.*, 2005, 2012] with Rice Convection Model in highest resolution available from the Coordinated Community Modeling Center (CCMC) (5 min cadence and 1/8 R_E (Earth radius) at the inner boundary), using the measured

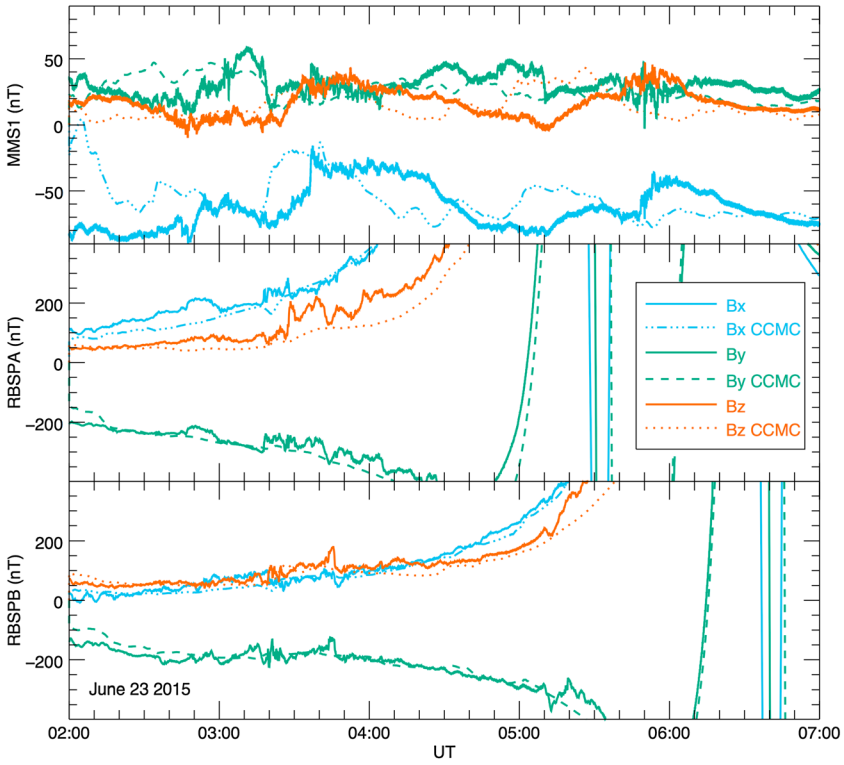

Figure 4. Tail magnetic fields observed by (top) MMS1 and Van Allen Probes (middle) A and (bottom) B (solid lines) and modeled (dashed lines) using a high-resolution run of BATS-R-US from the CCMC.

propagated solar wind and IMF from OMNIdata. The model showed many tail reconnection events in the time frame of 00:00 UT on 22 June to 24:00 UT on 23 June. Movies showing various cuts of the model for this event, including a cut that dynamically followed the MMS trajectory, can be found in the supporting information and at http://mms.rice.edu/June22. The model did especially well at capturing the several stretching and rapid dipolarizations observed in the 2–6 UT 23 June time frame (Figure 4, dashed). The first dipolarization in the model was between 3:15 and 3:20 (Figure 5a) and was observed at MMS at 3:16 [*Nakamura et al.*, 2016]. The second dipolarization in the model occurred between 04:55 and 05:00, seen at MMS at ~5:10 (see Movie S1 in the supporting information). The magnitude of the field changes predicted along the MMS path was quantitatively accurate, but with some variances in timing, reaching peak values somewhat earlier than measured. The model suggests that at the times of the dipolarizations, an X line is just downstream of MMS, which is very near the separatrix (Figure 5a). Since the tail was so stretched, a modest flapping of the tail affects the location of MMS relative to the model. The dipolarization signatures observed at VAP RBSP-A (Figure 4, middle) were accurate in location but low in amplitude. The dipolarization signatures observed at RBSP-B (Figure 4, bottom) showed good agreement both in magnitude and location. Thus, we argue that the O^+ ions seen flowing downstream in the lobe near the edge of the plasma sheet may be captured by the reconnection process and become the energetic O^+ seen in the plasma sheet.

When mapped to the ionosphere, the model showed extremely large field-aligned currents (FAC). As compared to the FAC's inferred from the AMPERE data [e.g., *Coxon et al.*, 2014], which reached an integrated value of nearly 25 MA, the predicted magnitudes were 20–50% smaller than that observed, although the timing structure was quite accurate (Figures 2e and 2f).

5. Polar Cap Convection Patterns

Because of the large magnetic field strengths (~40 nT) and the large and variable IMF *y* component, the model-predicted ionospheric convection varied from normal two-cell convection patterns during times of

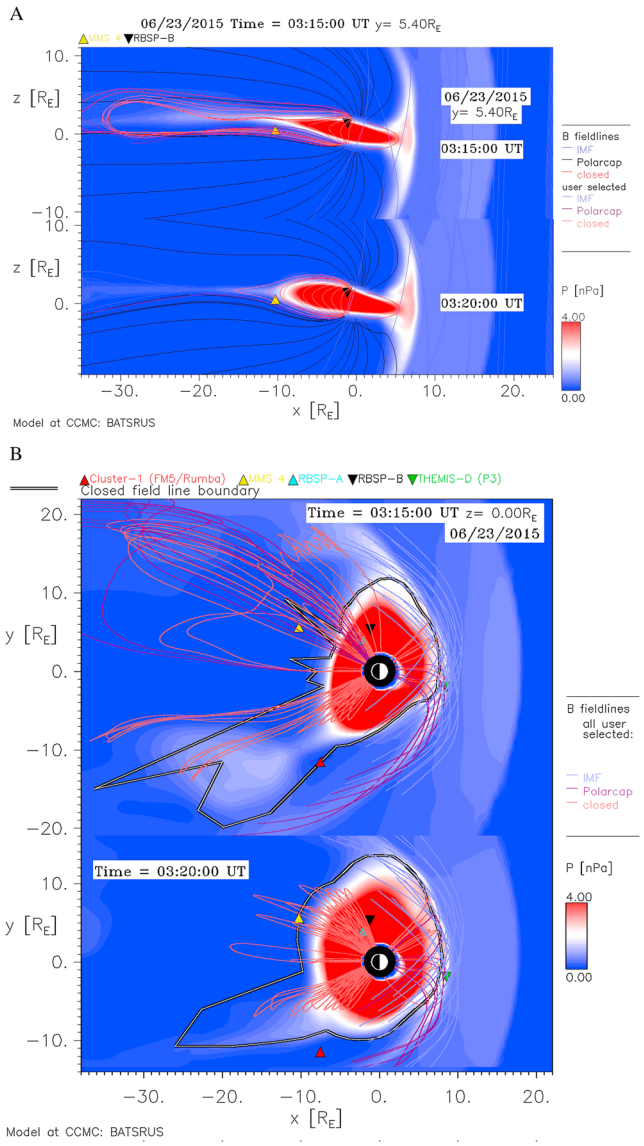

Figure 5. (a) Two frames from a movie of the CCMC run, showing MMS 1 spacecraft located very near the separatrix of an X line in the magnetotail. The dipolarization in the model is well observed between the stretched configuration of 03:15 and the more dipolar configuration of 03:20. The full movie including similar frames for the 05:00 dipolarization is in the supporting information and is available at http://mms.rice.edu/June22/. (b) Similar to Figure 5a, but showing the equatorial plane locations of the various magnetospheric spacecraft (MMS, VAP A and B, THEMIS, and Cluster) at the time of the dipolarization. The field lines in both times were started at the same locations on the equatorial plane. Note how less stretched each field line is after the dipolarization. A movie of this view is provided in the supporting information and on our website http://mms.rice.edu/June22.

large negative B_z (Figure 6a), to a four cell during high-positive IMF B_z intervals (Figure 6b) to a single convection cell rotating in opposite directions (clockwise in the North, counterclockwise in the South) in the two hemispheres after a long interval of strong + B_y (Figure 6c). A true single-cell convection pattern is very rare: in this case the single cell was only predicted (and observed) in the North. A movie of the modeled convection patterns (Movie S2) is part of the supporting information and posted at http://mms.rice.edu/June22.

A comparison with DMSP plasma flow data from the same intervals confirms the basic features of the convection, but interesting differences are observed. For example, in the southward IMF case (Figure 6a), the polar cap is larger in the data than in the model by about 5°. The sunward flow channel in the data during northward IMF (Figure 6b) is much narrower than in the model, which predicts a very large area of sunward flow in

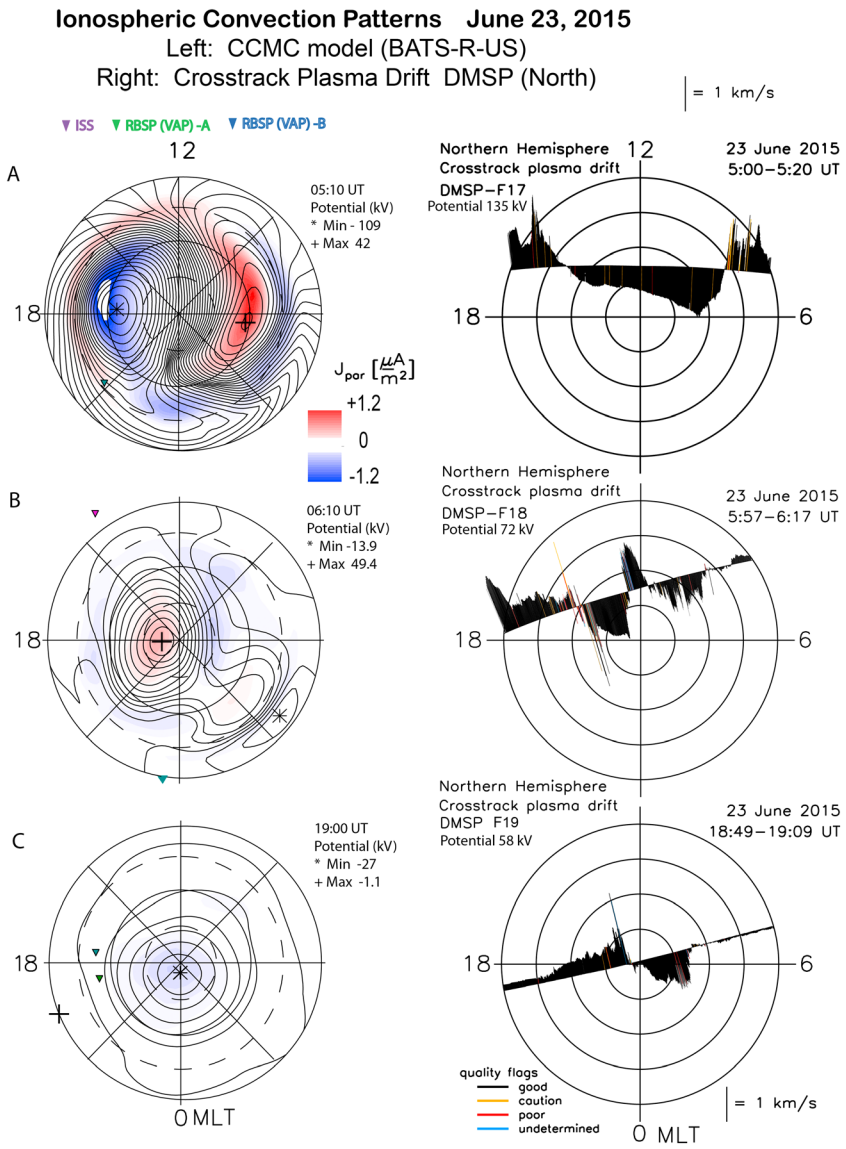

Figure 6. Northern polar cap convection equipotentials predicted from the BATS-R-US run (left image in each row). Colored areas are the field-aligned current densities, and equipotential lines are 4 kV apart in each plot. The movie is available at http://mms.rice.edu/June22 and in the supporting information. (right column) The measured cross-track plasma drifts from DMSP at the same time as the predicted potentials. (a) A normal two-cell convection pattern during southward IMF, (b) a four-cell pattern with reversed flow in the central polar cap during strong northward IMF, (c) a single-cell clockwise convection observed during strong positive *Y* component of the IMF.

the polar cap. The model also missed the strong low-latitude sunward flows on the dusk side. The DMSP flow data confirm the presence of a single-cell convection pattern in the North (Figure 6c, right), with just a hint of a viscous cell at 7 MLT, 75 ILAT. The cross-polar cap potential drops estimated from the model and from the flow data are comparable. Both the model and the data show the center of the cell just duskward of the magnetic pole [*Reiff and Burch*, 1985]. The lobe cell convection is more common in times of high sunward dipole tilt [*Crooker*, 1992], and this event, which occurred on 22–23 June, had maximum sunward tilt in the North.

6. Conclusions

This event represents the first major storm of the new Heliospheric Flotilla era. With well-instrumented spacecraft strategically placed in the magnetosphere, and new computational models, our understanding of

magnetospheric dynamics, especially its response during dramatic events such as the one presented in this paper, is taking a leap forward. Despite this being an anomalously intense event with large magnetic fields, the BATS-R-US model did an admirable job of reproducing the amount of field change during the dipolarizations, estimating the polar cap convection and currents, and the approximate location of MMS near the separatrix during a very dynamic magnetotail sequence.

Acknowledgments

The authors thank the MMS team for an amazing suite of instruments and for making high-resolution data available even during the commissioning phase. This work was carried out using the SWMF/BATS-R-US tools developed at The University of Michigan's Center for Space Environment Modeling (CSEM) and made available through the NASA Community Coordinated Modeling Center (CCMC). We particularly thank M. Kuznetsova for her help in optimizing the inputs. We thank Craig Kletzing for VAP magnetometer data, and the ACE team for plasma and IMF data through CDAWeb. This study was partially supported by the NASA MMS mission under contract 599790Q from SWRI to Rice University. It was also partially supported by NASA under grant NNX14AN55G to Rice University and WBS 943396.05.03.02.10.02 to Marshall Space Flight Center. The DMSP analysis was funded by NSF under grant AGS-1259508. All MMS data are now freely available to the community. Animations from the modeling runs are posted at http://mms.rice.edu/June22. The CCMC run is archived at http://ccmc.gsfc.nasa.gov/results/viewrun.php?

References

Baker, D. N., et al. (2016), A telescopic and microscopic examination of acceleration in the June 2015 geomagnetic storm: Magnetospheric Multiscale and Van Allen Probes study of substorm particle injection, *Geophys. Res. Lett.*, *43*, 6051–6059, doi:10.1002/2016GL069643.

Bala, R., and P. H. Reiff (2012), Improvements in short-term of geomagnetic Activity, *Space Weather*, *10*, S06001, doi:10.1029/2012SW000779.

Bala, R., and P. H. Reiff (2014), Validating the Rice neural network and the Wing *Kp* realtime models, *Space Weather*, *12*, 417–425, doi:10.1002/2014SW001075.

Burch, J. L., T. E. Moore, R. B. Torbert, and B. L. Giles (2016), Magnetospheric multiscale overview and science objectives, *Space Sci. Rev.*, doi:10.1007/s11214-015-0164-9.

Coxon, J. C., S. E. Milan, L. B. N. Clausen, B. J. Anderson, and H. Korth (2014), The magnitudes of the regions 1 and 2 Birkeland currents observed by AMPERE and their role in solar wind-magnetosphere-ionosphere coupling, *J. Geophys. Res. Space Physics*, *119*, 9804–9815, doi:10.1002/2014JA020138.

Crooker, N. U. (1992), Reverse convection, *J. Geophys. Res.*, *97*, 19,363–19,372, doi:10.1029/92JA01532.

Liao, J., L. M. Kistler, C. G. Mouikis, B. Klecker, I. Dandouras, and J.-C. Zhang (2010), Statistical study of O^+ transport from the cusp to the lobes with Cluster CODIF data, *J. Geophys. Res.*, *115*, A00J15, doi:10.1029/2010JA015613.

Liao, J., L. M. Kistler, C. G. Mouikis, B. Klecker, and I. Dandouras (2012), Solar cycle dependence of the cusp O^+ access to the near-Earth magnetotail, *J. Geophys. Res.*, *117*, A10220, doi:10.1029/2012JA017819.

Lu, G., P. H. Reiff, T. E. Moore, and R. A. Heelis (1992), Upflowing ionospheric ions in the auroral region, *J. Geophys. Res.*, *97*, 16,855–16,863, doi:10.1029/92JA01435.

McComas, D. J., S. J. Bame, P. Barker, S. C. Feldman, J. L. Phillips, P. Riley, and J. W. Griffee (1998), Solar Wind Electron Proton Alpha Monitor (SWEPAM) for the Advanced Composition Explorer, *Space Sci. Rev.*, *86*, 613, doi:10.1023/A:1005040232597.

Nakamura, R., et al. (2016), Transient, small-scale field-aligned currents in the plasma sheet boundary layer during storm time substorms, *Geophys. Res. Lett.*, *43*, 4841–4849, doi:10.1002/2016GL068768.

Pollock, C., et al. (2016), Fast Plasma Investigation for magnetospheric multiscale, *Space Sci. Rev.*, doi:10.1007/s11214-016-0245-4.

Powell, K. G., P. L. Roe, T. J. Linde, T. I. Gombosi, and D. L. De Zeeuw (1999), A solution-adaptive upwind scheme for ideal magnetohydrodynamics, *J. Comput. Phys.*, *154*, 284–309.

Reiff, P. H., and J. L. Burch (1985), By-dependent plasma flow and Birkeland currents in the dayside magnetosphere: 2. A global model for southward and northward IMF, *J. Geophys. Res.*, *90*, 1595–1609, doi:10.1029/JA090iA02p01595.

Russell, C. T., et al. (2016), The magnetospheric multiscale magnetometers, *Space Sci. Rev.*, doi:10.1007/s11214-014-0057-3.

Smith, C. W., J. L'Heureux, N. F. Ness, M. H. Acuña, L. F. Burlaga, and J. Scheifele (1998), The ACE magnetic fields experiment, *Space Sci. Rev.*, *86*, 613, doi:10.1023/A:1005092216668.

Tóth, G., et al. (2005), Space Weather Modeling Framework: A new tool for the space science community, *J. Geophys. Res.*, *110*, A12226, doi:10.1029/2005JA011126.

Tóth, G., et al. (2012), Adaptive numerical algorithms in space weather modeling, *J. Comput. Phys.*, *231*, 870–903, doi:10.1016/j.jcp.2011.02.006.

Young, D. T., et al. (2016), Hot plasma composition analyzer for the magnetospheric multiscale mission, *Space Sci. Rev.*, doi:10.1007/s11214-014-0119-6.